Supercapacitive Properties of Symmetry and the Asymmetry Two Electrode Coin Type Supercapacitor Cells Made from MWCNTS/Nickel Oxide Nanocomposite

Abolanle S. Adekunle[1, 2], Kenneth I. Ozoemena[3, 4], Bhekie B. Mamba[1], Bolade O. Agboola[5,*],
Oluwafemi S. Oluwatobi[6]*

[1] Department of Chemical Technology, University of Johannesburg, P.O. Box 17011, Doornfontein, 2028, South Africa
[2] Department of Chemistry, Obafemi Awolowo University, Ile-Ife, Nigeria
[3] Department of Chemistry, University of Pretoria, Pretoria, South Africa
[4] Energy & Processes Unit, Materials Science and Manufacturing, Council for Scientific and Industrial Research (CSIR), Pretoria, South Africa
[5] Department of Petroleum Chemistry and Engineering, American University of Nigeria, Yola, Nigeria
[6] Department of Chemistry and Chemical Technology, Walter Sisulu University, Mthatha Campus, Mthatha E. Cape South Africa
[*] E-mail: sadek2k@yahoo.com, bolade.agboola@aun.edu.ng

Supercapacitive properties of synthesised nickel oxides (NiO) nanoparticles integrated with multi-walled carbon nanotubes (MWCNT) in a two-electrode coin cell type supercapacitor were investigated. Successful formation of the MWCNT-NiO nanocomposite was confirmed with techniques such as transmission electron microscopy (TEM), scan electron microscopy (SEM), electron dispersive X-ray spectroscopy (EDX) and X-ray diffraction spectroscopy (XRD). The supercapacitance behaviour of both the symmetry and the asymmetry MWCNT-NiO based supercapacitor in 1 M H_2SO_4 and 1 M Na_2SO_4 electrolytes was evaluated using cyclic voltammetry (CV), electrochemical impedance spectroscopy (EIS) and galvanostatic constant current charge-discharge (CD) techniques. There was a good correlation between the CV and the CD specific capacitance (SC) values for the asymmetry supercapacitor. Asymmetry supercapacitor (MWCNT-NiO|H_2SO_4|MWCNT) gave the highest SC value of 925.9 mFcm^{-2} (53.9 F g^{-1}). High SC values which are higher than most of those reported in literature were obtained. The electrodes demonstrated high stabilities with no significant changes in SC values over 1000 cycles.

Keywords: MWCNT-nickel oxide nanocomposite; Electrochemical Impedance; Galvanostatic charge-discharge; Symmetry, Asymmetry

1. INTRODUCTION

Studies have shown that carbon nanotubes-metal oxide (CNT/MO) nanocomposite modified electrodes exhibited huge capacitive current in some electrolytes [1,2]. Therefore, it becomes imperative to establish the charge storage properties of these materials as a potential source for energy generation. This is in response to the increasing demands for clean energy technologies, where supercapacitors are considered to be the most promising energy storage and power output technologies [3] for portable electronics, electric vehicles, and renewable energy systems. Supercapacitors also fill the gap between batteries and conventional dielectric capacitors and have considerable potential for use in high power applications [4]. They are classified as either double-layer or pseudo-capacitors. Double-layer capacitors stores charges through non-faradaic processes while the pseudo-capacitors are through faradaic process.

Carbon based supercapacitor electrodes have been attractive due to their high surface area and porous nature [5-11]. Recently, both single-walled and multiwalled carbon nanotubes (SWNT and MWNT) have been recognized as potential electrode materials for electrochemical supercapacitors, owing to their special properties such as high chemical stability, low mass density, low resistivity, narrow distribution of mesopore sizes, and large surface area [12,13]. Several transition metal oxides have been used as supercapacitor materials such as anhydrous Co–Ni oxides [14], MnO_2 or MnOx [15,16], NiO [17,18], Co_3O_4 [19], and Fe_3O_4 [20], but RuO_2 is well known as a good metal oxide in supercapacitors because of its high specific capacitance values (740 F g^{-1}) [21] even though its application is limited due to its high cost and toxicity. Transition metal oxides attached to CNTs have been studied recently and are expected to show improved capacitive behaviour due to their enhanced stability and high conductivity [22]. Thus, the hybrid of an electric double layer system and a Faradaic pseudocapacitive system could be a good candidate for a supercapacitor with high specific capacitance and energy density [5].

In this work, we established the supercapacitive behaviour of synthesised nickel oxides supported on MWCNT platform in acidic and neutral medium using two-electrode asymmetric and symmetric systems in a coin type supercapacitor cell. Our study was prompted by the paucity of literature on the supercapacitive properties of NiO modified electrode in acidic medium in comparison to alkaline medium and also, the fact that asymmetric supercapacitors exhibit better capacitive rate behaviour compared to the symmetrical ones [23]. Our findings showed that the acid-functionalised MWCNTs significantly enhanced the supercapacitance of the synthesised nickel oxide in the media studied, as compared to other literature reports.

2. EXPERIMENTAL

2.1. Materials and Reagents

Multi-walled carbon nanotubes (MWCNTs), obtained from Aldrich, was acid-digested using the known procedure [24]. $NiNO_3.6H_2O$ and Na_2SO_4 were obtained from Sigma-Aldrich chemicals.

Ultra pure water of resistivity 18.2 MΩcm was obtained from a Milli-Q Water System (Millipore Corp., Bedford, MA, USA) and used throughout for the preparation of solutions. A phosphate buffer solution (PBS, pH 7.0) was prepared with appropriate amounts of K_2HPO_4 and KH_2PO_4, and the pH adjusted with 0.1 M H_3PO_4 or NaOH. All electrochemical experiments were performed with nitrogen-saturated phosphate buffer solution (PBS). All other reagents were of analytical grades and were used as received from the suppliers without further purification.

2.1.1. Syntheses of nickel oxide nanoparticles

Nickel oxide (NiO) nanoparticles were prepared using the method described by Xiang et al. [25]; 100 mL of precipitation solution (NH_4HCO_3) was dropped at the rate of 5.0 mL min^{-1} into 50 mL of 0.5 M Ni^{2+} solution. During precipitation, the suspension was kept at constant temperature (40 ^{0}C), and constant stirring (800 rpm) for 1 h. The precipitate formed was washed with distilled water and copious amount of ethanol several times to remove possible adsorbed ions such as Ni^{2+}, NH_4^+, Cl^-, NO_3^-, CO_3^{2-}, and OH^-. The precipitate was oven-dried at 105 ^{o}C for 12 h, and later heated in air at 400 ^{o}C for 1 h. The product was pulverised and used for analysis.

2.2. Equipment and Procedure

High resolution field emission scanning electron microscopy (HRSEM) images were obtained with Zeiss Ultra Plus Oberkochem (Germany), transmission electron microscopy (TEM) experiment was performed using a Model JEOL JEM-2100F field emission transmission electron microscope, Tokyo (Japan) while the energy dispersive X-ray spectra were obtained from NORAN VANTAGE (USA). The XRD analysis was done using a back loading preparation method. The sample was analysed using a PANanalytical X'Pert Pro powder diffractometer (Netherland) with X'Celerator detector and variable divergence- and receiving slits with Fe filtered Co-Kα radiation. Electrochemical experiments were carried out using an Autolab Potentiostat PGSTAT 302 (Eco Chemie, Utrecht, The Netherlands) driven by the GPES software version 4.9. Electrochemical impedance spectroscopy (EIS) measurements were performed with Autolab Frequency Response Analyser (FRA) software between 10 mHz and 100 kHz using a 5 mV rms sinusoidal modulation in the electrolyte solutions at 0.55 and 0.75 V vs. Ag|AgCl, sat'd KCl). ISE ORION meter, model 420A, was used for pH measurements. Experiments were performed at 25±1 °C.

2.3. Electrode Preparation: Coin type cell assembly

The electrochemical performance of the prepared powder of MWCNT-NiO nanocomposite made by chemical synthesis was investigated using two-electrode coin-type cells (CR 2032) with steel foil as reference electrode. The working electrode was assembled by coating the slurry of the MWCNT-NiO on an aluminium foil current-collector of 12 mm in diameter. The mixture composed of 71.4 wt. % active material, 14.3 wt. % functionalised MWCNT and 14.3 wt. % binder (polyvinylidene

fluoride) in an N-methylpyrrolidione (NMP) solvent. After drying in an oven at 80°C for 2 h, the electrodes were pressed under a pressure of 7MPa for 1min. The weight of the active materials was determined by weighing the Al foil before and after pressing the powders. The supercapacitive behaviour was investigated in both acidic (1 M H_2SO_4) and neutral (1 M Na_2SO_4) electrolytes. In the symmetric assembly, MWCNT-NiO was used as both the positive and the negative electrode. In the asymmetry assembly, the working electrode (MWCNT-NiO) was used as the positive electrode while the MWCNT alone was used as the negative electrode. The electrodes were soaked in the electrolyte for about 10 mins before assembled in the coin cells. A polypropylene (PP) film (Cellgard 2400) was used as the separator.

3. RESULTS AND DISCUSSION

3.1. Comparative FETEM, HRSEM, EDX and XRD

Figure 1a and b are the typical TEM for the MWCNT-Ni and the MWCNT-NiO nanocomposite, while Fig. 1c and d are their corresponding HRSEM images, showing the transformation in the morphology of the synthesised Ni to the NiO nanoparticles. The MWCNT-Ni nanoparticles are porous and somewhat aggregated, possibly due to the strong electrostatic interactions between the metal ions and the COO^- charge of the acid-treated MWCNTs while MWCNT-NiO nanoparticles appeared crystalline with mono-disperse particles along the MWCNTs. The particle sizes are in the 10 – 30 nm range from the TEM pictures.
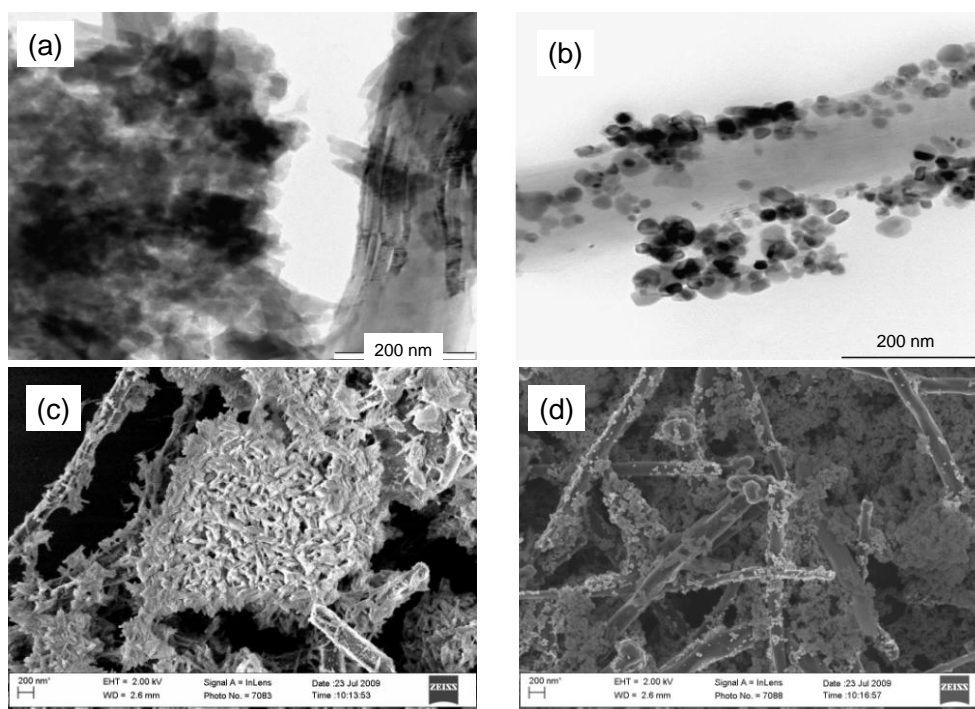

Figure 1. FETEM images of (a) MWCNT-Ni, (b) MWCNT-NiO nanocomposite. (c) and (d) are their respective HRSEM images.

Figure 2 is the EDX profile of the MWCNT-Ni and the MWCNT-NiO modified electrodes. The presence of Ni peak in (a) and (b) showed that the electrodes were successfully modified with the Ni nanoparticles. More importantly, the pronounced relative intensity of the oxygen peak in (b) confirmed the oxide form of the metal. The trace oxygen peak in (a) and the carbon peaks in (a) and (b) have been attributed to the functionalised MWCNT-COOH.
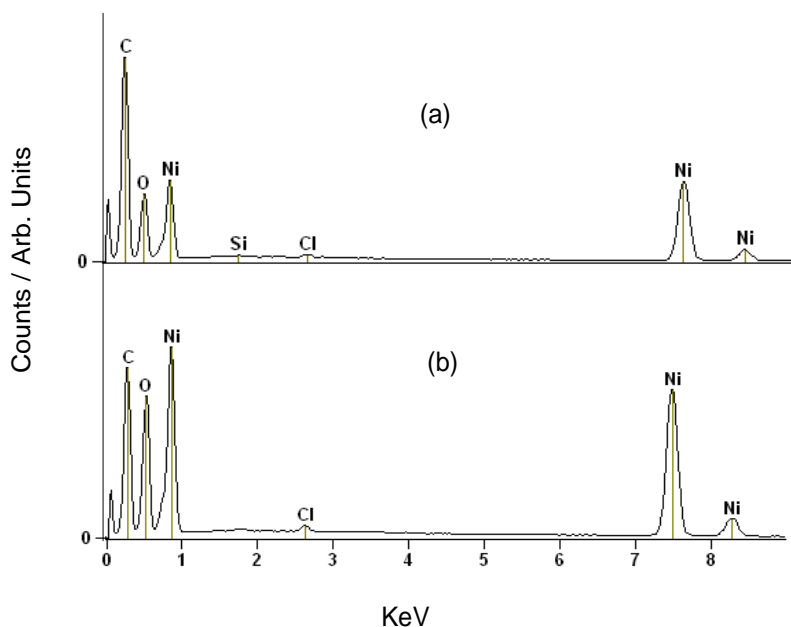

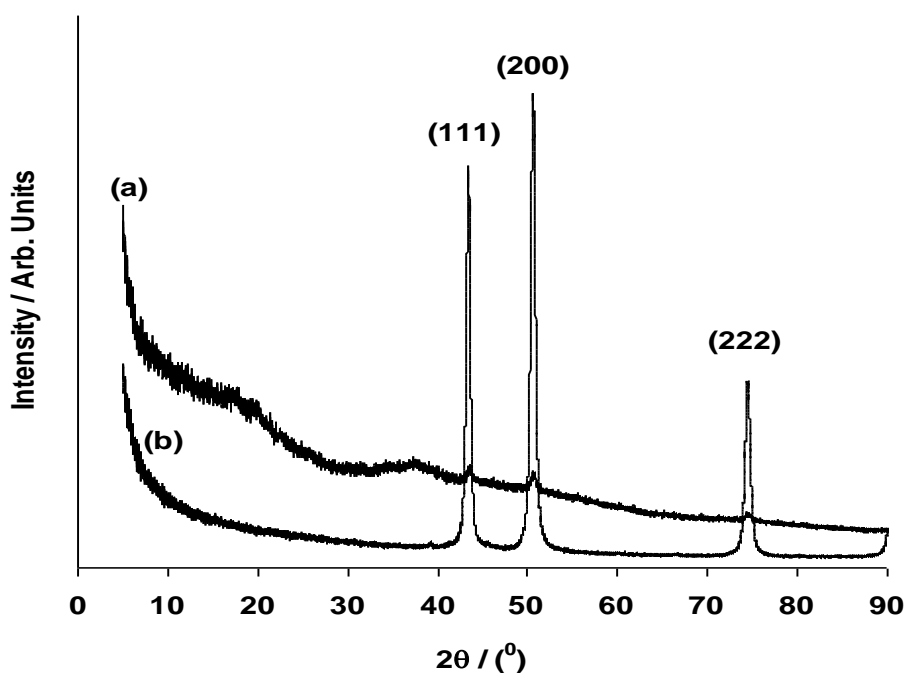**Figure 2.** EDX spectra of (a) MWCNT-Ni and (b) MWCNT-NiO nanocomposite.

Figure 3. XRD spectra of the synthesised (a) Ni and (b) NiO nanoparticles.

The corresponding XRD spectra for the Ni (a) and the NiO (b) particles are shown in Figure 3. The XRD of the Ni particles appeared amorphous with a broad Ni peak at about 2θ of 38^0. Three characteristic peaks for NiO (2θ = 43.4, 50.6 and 74.5), corresponding to Miller indices (111), (200) and (222) were observed and indicates that the resultant particles were pure face-centered cubic (fcc) nickel [26]. From Debye-Scherrer formula [27], the average crystal size of the NiO nanoparticles were calculated to be ~ 21.5 nm, this value collaborate the calculated particle size range of 10-30 nm obtained from TEM.

3.2. Comparative cyclic voltammetry experiments of the two coin cell based supercapacitors

Figure 4 presents the cyclic voltammograms obtained for the symmetry (a) and (b); and the asymmetry (c) and (d) MWCNT-NiO based supercapacitor in 1 M H_2SO_4 and 1 M Na_2SO_4 aqueous electrolyte respectively at scan rate 5, 25, 50, 100, 200, 300, 400 and 500 mVs^{-1} (i-viii, inner to outer).
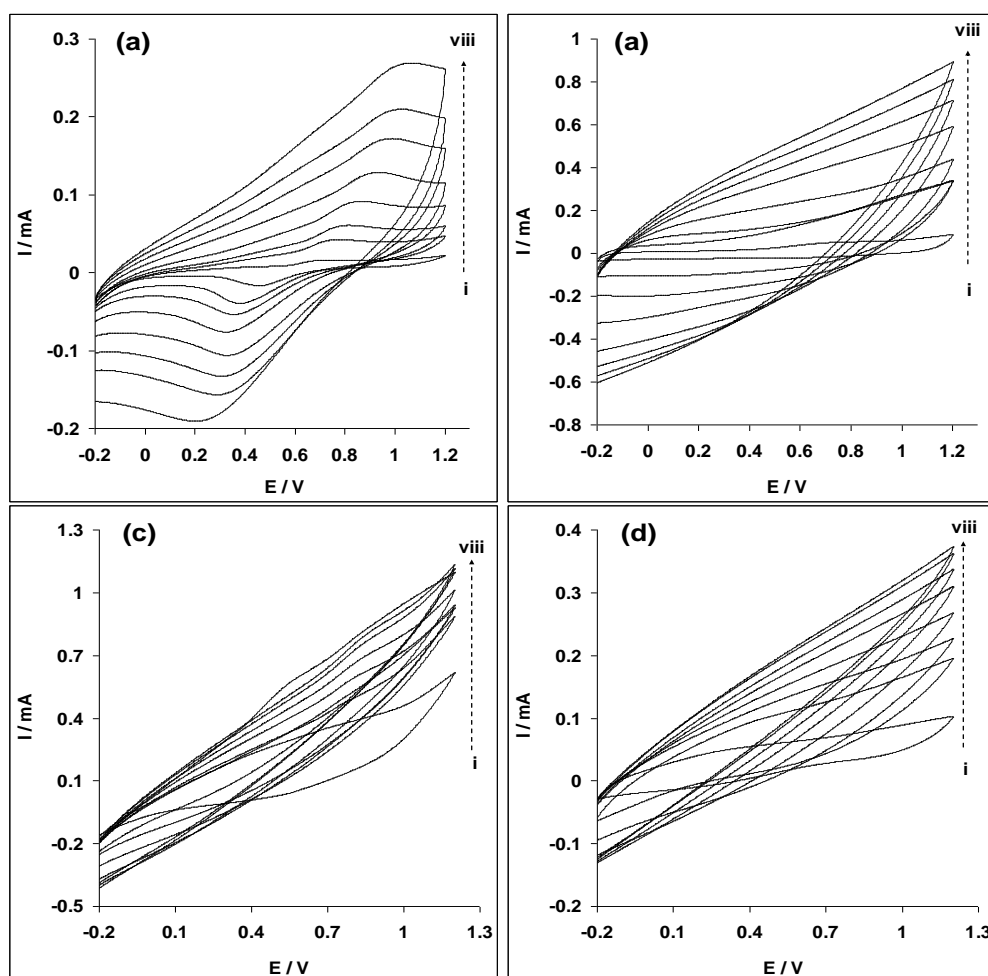

Figure 4. Cyclic voltammograms obtained for the symmetry (a) and (b); and the asymmetry (c) and (d) MWCNT-NiO based supercapacitor (two–electrode cell) in 1 M H_2SO_4 and 1 M Na_2SO_4 aqueous electrolyte respectively at scan rate 5, 25, 50, 100, 200, 300, 400 and 500 mVs^{-1} (i-viii, inner to outer); mass of each electrode, 1.4 mg.

For the symmetric based electrode in acidic medium (Fig. 4a), there is a redox peaks at $E_a \sim$ 0.80 V and $E_c \sim$ 0.40 V (scan rate 5 m s^{-1}) due to the Ni(II)/Ni(III) redox process. The ratio of the anodic and the cathodic current (I_{pa}/I_{pc}) is 1.0, which implies a favoured reversible or charge/discharge process of the supercapacitor material. On the other hand, in H_2SO_4, the asymmetry base supercapacitor showed a broad anodic peak at a lower potential ($E_a \sim$ 0.57) and, a weak and broad cathodic peak at *ca* 0.50 V (Fig. 4c).

Table 1. Specific capacitance (mFcm^{-2}) for the symmetric and asymmetric MWCNT-NiO based supercapacitor (two-electrode cell) in 1 M H_2SO_4 and 1 M Na_2SO_4 aqueous electrolyte respectively. Values in parenthesis are the specific capacitance in F/g.

Scan rate (mVs^{-1})	Specific capacitance (Asymmetrical)		Specific capacitance (Symmetrical)	
	MWCNT-NiO|H_2SO_4|NiO-MWCNT	MWCNT-NiO|H_2SO_4|MWCNT	MWCNT-NiO|Na_2SO_4|NiO-MWCNT	MWCNT-NiO|Na_2SO_4|MWCNT
5	80.0 (4.6)	950.0 (54.3)	194.0 (11.1)	220.0 (12.6)
25	40.0 (3.2)	450.0 (25.7)	152.0 (8.7)	92.0 (5.3)
50	27.5 (2.2)	160.0 (9.1)	110.0 (6.3)	47.5 (2.7)
100	21.2 (1.2)	65.0 (3.7)	62.5 (3.6)	30.0 (1.7)
200	15.0 (0.9)	41.6 (2.4)	47.5 (2.7)	16.3 (0.93)
300	12.5 (0.72)	29.6 (1.7)	34.2 (2.0)	11.7 (0.7)
400	11.9 (0.68)	24.6 (1.4)	30.6 (1.8)	10.0 (0.6)
500	12.0 (0.68)	21.4 (1.2)	28.0 (1.6)	7.0 (0.4)

However as scan rate increases, the cathodic peak disappears while the anodic peak shift with increasing scan rate indicating a high capacitive behaviour. As scan rate increases, a large current separation with mirror images are observed at higher scan rate for both the symmetry and asymmetry supercapacitors. The CVs tend to be rectangular in H_2SO_4 than in Na_2SO_4 but the lack of perfect rectangular shape for the curves in both cases is attributed to the combination of double layer and pseudo-capacitances contributing to the total capacitance [28]. The specific capacitance (SC) was estimated from the cyclic voltammograms using the Equation 1:

$$C_{film} \ (Fcm^{-2}) = \frac{I_{ch}}{vA} \qquad (1)$$

where I_{ch} is the average charging current, v the scan rate and A is the area of the electrode active material in cm^2. The capacitance values decreases with increasing scan rate (Table 1.0). The highest SC values of 80 and 194 mFcm^{-2} (for the symmetry); and 950 and 220 mFcm^{-2} (for the

asymmetry) supercapacitors were obtained in 1 M H_2SO_4 and 1 M Na_2SO_4 respectively at scan rate of 5 mVs^{-1}.

The specific capacitance per mass of one cell electrode was calculated according to the Equation 2 [28]:

$$SC \ (F/g) = 2\frac{C}{m} \qquad (2)$$

Where *C* is the experimental measured capacitance of the supercapacitor, m is the mass of one composite electrode. The specific capacitance in F/g is represented in parenthesis in Table 1.0. From Table 1, our result agreed with other reports where it was established that the asymmetry assembly exhibit higher specific capacitance values than their symmetry counterpart [23, 29-31]. The results followed the same trend with those obtained by Ganesh et al. [30] however the highest value of 960 mFcm^{-2} obtained at 5 mVs^{-1} was quite significantly higher than the 83 mFcm^{-2} obtained (at the same scan rate) for asymmetric supercapacitor cell assembly based on NiO in 6 M KOH [30]. The difference can be attributed to the different methods of obtaining the supercapacitor material and the well conducting and the mesoporous nature of functionalised MWCNT in enhancing charge flow in the nanocomposite used in this study. The equivalent specific capacitance value of 54.3 F/g at 5 mVs^{-1} obtained in this study is also greater compared to 34 and 27.67 F/g obtained at 2 and 5 mVs^{-1} respectively for an asymmetric NiO supercapacitor cell assembly in 6 M KOH electrolyte [30].

3.3 Electrochemical impedance studies

To further examine the detailed electrical properties or capacitive behaviour of the MWCNT-NiO electrodes in the electrolytes, electrochemical impedance spectroscopy (EIS) experiment was conducted at $E_{1/2}$ of 0.55 V vs Ag|AgCl, sat'd KCl. Figure 5a presents the Nyquist plots obtained for the symmetry and the asymmetry assembly in both electrolytes. The Nyquist plots showed a good capacitor-like behaviour with a small diffusion limitation. Figure 5b to d are the equivalent electrical circuits' diagrams for fitting of the impedance data.

In the circuits, R_s represents the solution/electrolyte resistance (R_s), R_{ct} is the charge-transfer resistance, *C* is the double layer capacitance of the electrode (C_{dl}), Z_w is the Warburg impedance relating to the semi-infinite linear diffusion and *Q* or *CPE* represents the pseudocapacitance or the porous nature of the electrode. The data obtained from the fittings are presented in Table 2, clearly showing satisfactory fitting as judged by the low relative errors.

Circuit 5b fitted impedance data obtained for the symmetry assembly in both 1 M H_2SO_4 and 1 M Na_2SO_4 (Table 2). Circuits 5c and 5d fitted the impedance data for the asymmetry assembly in 1 M H_2SO_4 and 1 M Na_2SO_4 electrolytes respectively (Table 2). From the Table, the assymetry supercapacitor, MWCNT-NiO|H_2SO_4|MWCNT has the lowest R_{ct} values (1.28 Ωcm^{-2}) in 1 M H_2SO_4. The result indicates faster charge transport of the supercapacitor, which also could be responsible for its high SC values.
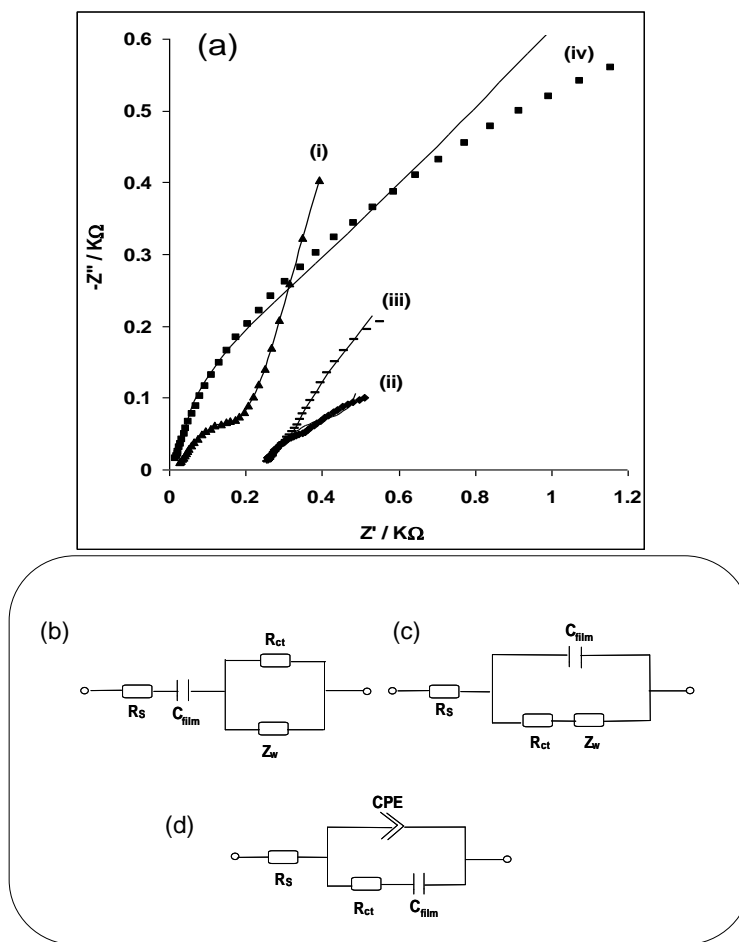
Figure 5. (a) Typical Nyquist plots obtained for the symmetry: (i) MWCNT-NiO|H$_2$SO$_4$|MWCNT-NiO, (ii) MWCNT-NiO|Na$_2$SO$_4$|MWCNT-NiO; and the asymmetry: (iii) MWCNT-NiO|H$_2$SO$_4$|MWCNT and (iv) MWCNT-NiO|Na$_2$SO$_4$|MWCNT supercapacitors at a fixed potential of 0.55 V vs Ag|AgCl sat'd KCl. The square data points are experimental while the solid lines in the spectra represent non-linear squares fits. Figure 5b-d is the circuit used for fitting of the impedance data in (a).

A phase angle of 31^0 and 11^0 were obtained for the symmetry assembly supercapacitors (MWCNT-NiO|H$_2$SO$_4$|MWCNT-NiO) and (MWCNT-NiO|Na$_2$SO$_4$|MWCNT-NiO), indicating a pseudocapacitive behaviour. Similar pseudocapacitive behaviour was obtained for the asymmetry assembly supercapacitors (MWCNT-NiO|H$_2$SO$_4$|MWCNT) and (MWCNT-NiO|Na$_2$SO$_4$|MWCNT) with phase angles of 21° and 52° respectively. A phase angle of 90° is expected for pure and ideal capacitive behaviour.

The low-frequency differential capacitance (C_d) for each of the electrodes can be obtained from the slope ($1/2\pi C_d$) of the plot of the imaginary component of the impedance versus the reciprocal of the frequency (i.e., *-Z"* vs $1/f$). The values of the C_d for the symmetric and the asymmetric electrodes in 1 M Na$_2$SO$_4$ and H$_2$SO$_4$ were much smaller than values obtained using the galvanostatic discharge method.

Table 2. Impedance data obtained for the symmetry and asymmetry MWCNT-NiO nanocomposite based supercapacitor (two-electrode cell) in 1.0 M H_2SO_4 and 1.0 M Na_2SO_4 electrolytes at a fixed potential of 0.55 V vs. Ag|AgCl sat'd KCl.

Electrode	Impedimetric parameters					
	R_s (Ω cm^2)	C_{dl} ($\mu F cm^{-2}$)	R_{ct} (Ω cm^2)	CPE ($\mu F cm^{-2}$)	n	Z_w ($\mu\Omega$ cm^2)
MWCNT-NiO|H_2SO_4| MWCNT-NiO	2.15 ±0.03	1330.30 ±121.99	52.05 ±0.64	-	-	11.63 ±0.12
MWCNT-NiO|Na_2SO_4| MWCNT-NiO	24.73 ±0.02	1100.00 ±156.00	30.94 ±0.10	-	-	8.85 ±0.04
MWCNT-NiO|H_2SO_4| MWCNT	25.69 ±0.02	4.90 ±0.78	1.28 ±0.01	-	-	23.79 ±0.05
MWCNT-NiO|Na_2SO_4| MWCNT	-2.39 ±0.04	0.70 ±0.04	9.42 ±0.12	1308.0 ±84.10	0.33 ±0.01	-

For example, the symmetry (MWCNT-NiO|H_2SO_4|MWCNT-NiO) gave approximately 3.58 and 2.58 mFcm^{-2} in 1 M H_2SO_4 and Na_2SO_4 while the asymmetry (MWCNT-NiO|H_2SO_4|MWCNT) gave values of 3.08 and 2.17 mFcm^{-2} in 1 M H_2SO_4 and Na_2SO_4 respectively. The discrepancy in the value can be attributed to the polymeric nature of the CNT [33] used as nanocomposite as such behaviour have been observed mainly for conducting polymers [30,34-42].

3.4 Comparative galvanostatic charge / discharge experiments

Galvanostatic charge-discharge is the most reliable and accurate method for evaluating the supercapacitance of electrodes because it gives closer estimation of close to the practical work of a capacitor. The comparative current charge/discharge experiment of the supercapacitor cell assembly in (a) 1 M H_2SO_4 and (b) 1 M Na_2SO_4 electrolyte solutions at current density of 0.25 mA cm^{-2} was studied at potential range of - 0.2 to 0.8 V in order to observe the pseudocapacitance arising from the redox reaction at this voltage range. Figure 6 (symmetry) and Figure 7 (asymmetry) represent the charge/discharge curve obtained in both electrolytes respectively. It was observed that the charging-discharging times are almost the same.

The specific capacitance of the supercapacitor (SC) was calculated using Equations 3 and 4 below [15]:

$$SC\ (Fcm^{-2}) = \frac{I \times \Delta t}{\Delta E \times A} \tag{3}$$

$$SC\ (Fg^{-1}) = \frac{I \times \Delta t}{\Delta E \times m} \tag{4}$$

where *I* is the discharge current in ampere, Δt is the discharge time in second, ΔE is the discharge voltage in volt, *A* and m are the area and the mass of the electrode active material in cm^2 or g respectively.
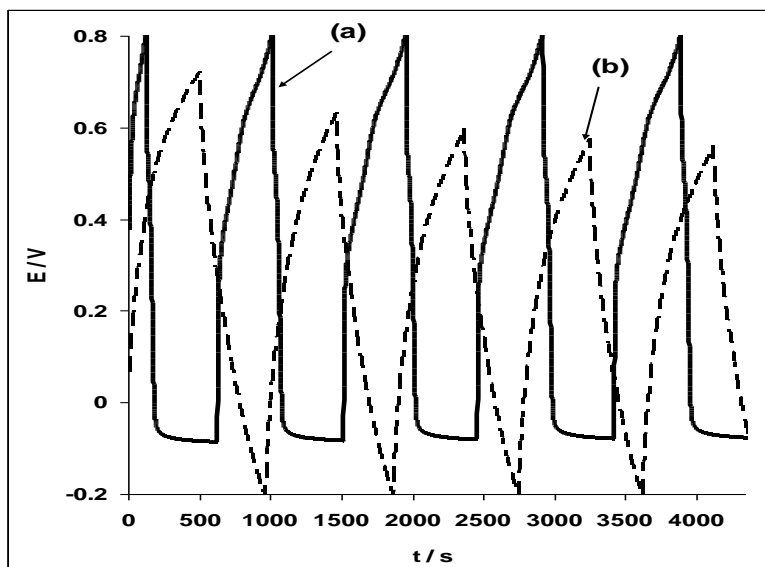

Figure 6. Typical examples of the galvanostatic charge discharge profile for the symmetry (MWCNT-NiO) based supercapacitor (two-electrode cell) in (a) 1 M H_2SO_4 and (b) 1 M Na_2SO_4 aqueous electrolytes, at an applied current density of 0.25 mAcm^{-2}.
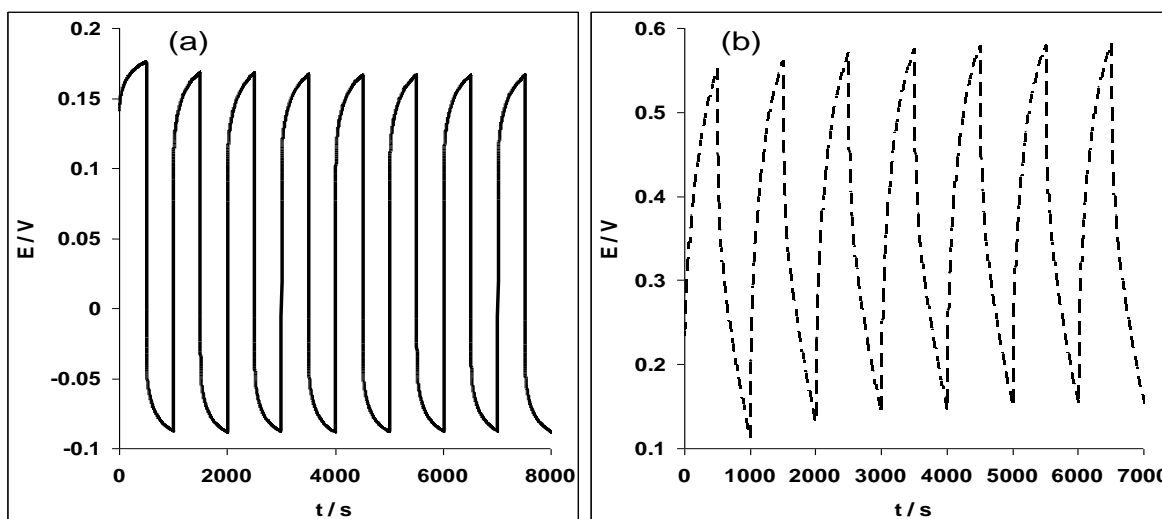

Figure 7. Typical examples of galvanostatic charge discharge profile of the asymmetry MWCNT-NiO based supercapacitor (two-electrode cell) in (a) 1 M H_2SO_4 and (b) 1 M Na_2SO_4 aqueous electrolytes, at an applied current density of 0.25 mAcm^{-2}.

The calculated SC is 277.8 mAcm^{-2} (or 7.8 F/g) and 255.0 mAcm^{-2} (or 7.2 F/g) for the symmetry supercapacitor in 1 M H_2SO_4 and 1 M Na_2SO_4 respectively. The values are higher, 925.9 mAcm^{-2} (53.9 F/g) and 568.2 mAcm^{-2} (15.9 F/g) for the asymmetry assembly in 1 M H_2SO_4 and 1 M

Na_2SO_4 respectively. The SC values obtained from the charge-discharge experiment are slightly higher especially for the symmetry supercapacitor compared with those obtained from the CV experiment but there is a good correlation between the CV and galvanostatic measurements for the asymmetry cell. The SC value (53.9 F/g) recorded for the asymmetry MWCNT-NiO|H_2SO_4|MWCNT supercapacitor in H_2SO_4 is higher compared with 37 and 40 F/g reported for the symmetry (NiO|KOH|NiO) and the asymmetry (NiO|KOH|activated carbon) supercapacitors respectively using same technique [30]. Aside the fact that the high capacitance of the MWCNT-NiO has been related to the possible consequence of its high surface area and quality pore networks, the higher SC values in H_2SO_4 observed in this study can also be attributed to the relatively small H^+ ion size which will expectedly make diffusion of H^+ ions into the pores of MWCNT-NiO|MWCNT easier.
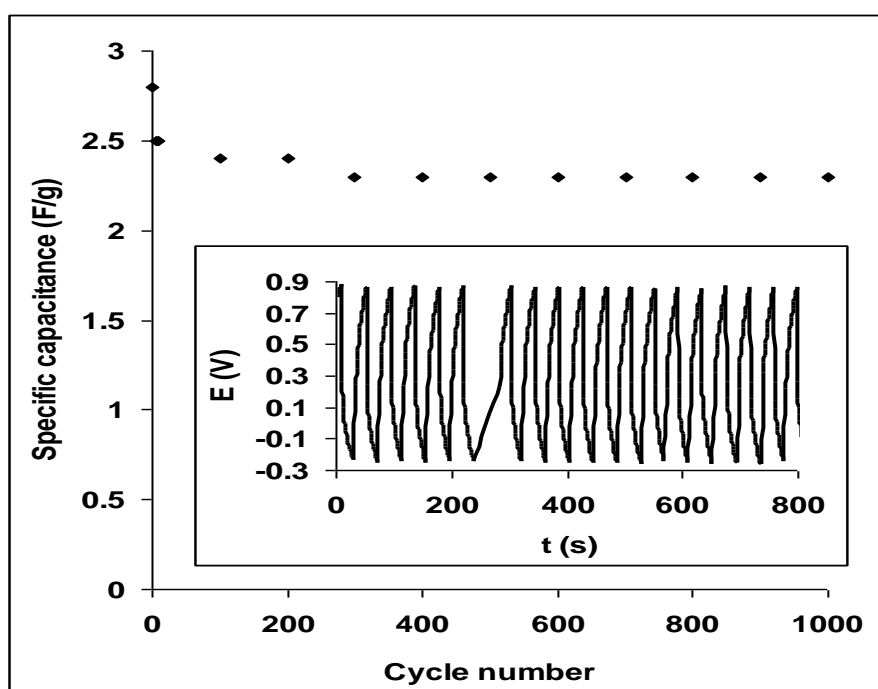

Figure 8. Cyclic life (1000 cycles) of the asymmetry MWCNT-NiO |H_2SO_4|MWCNT supercapacitor showing its cycle stability in 1 M H_2SO_4 aqueous electrolytes. Inset is the section of the charge-discharge curves obtained for the cell at applied current density of 2.5 mAcm^2.

The specific power density (SP) and specific energy (SE) were easily estimated from the discharge process using Equations 5 and 6 [15,43]:

$$SP\,(Wkg^{-1}) = \frac{I \times \Delta E}{m} \qquad (5)$$

$$SE\,(WhKg^{-1}) = \frac{I \times t \times \Delta E}{m} \qquad (6)$$

where all units retain their usual meaning. The SP and SE values of the best electrode film (MWCNT-NiO|H$_2$SO$_4$|MWCNT) are 3.8 Wkg^{-1} and 1.9 KWhKg^{-1} respectively. The energy deliverable efficiency (η / %) of the electrode was obtained from Equation 7 [43].

$$\eta \ (\%) = \frac{t_d}{t_c} \ \times \ 100 \qquad\qquad (7)$$

where t_d and t_c are discharge time and charging time, respectively. The energy deliverable efficiency for MWCNT-NiO|H$_2$SO$_4$|MWCNT is 101.0±8.1%.

Since the asymmetry MWCNT-NiO|H$_2$SO$_4$|MWCNT cell gave the highest capacitance, we investigated the stability of the cell at a current density of 2.5 mAcm^{-2}. A typical repetitive charge-discharge cycling for 1000 cycles, lasting about 24 h is shown in Figure 8. The electrode is able to charge and discharge continuously for over 900 cycles without any significant loss (< 5 %) in SC value. The electrode stability was attributed to the ease of diffusion of ions in and out of the porous nanocomposite structure and the chemical stability of the MWCNT, even against strong acid condition.

4. CONCLUSION

This study showed successful synthesis of NiO nanoparticles/multi-walled carbon nanotubes nanocomposite as confirmed by the different characterisation techniques such as HRSEM, FETEM, EDX and XRD. The SEM and TEM images also clearly indicated the porous nature of the MWCNT-NiO modified electrodes. There is a good correlation between the CV and galvanostatic measurements for the asymmetry supercapacitor. Cyclic voltammetry, electrochemical impedance spectroscopy and galvanostatic charge discharge techniques revealed that the asymmetry configuration; MWCNT-NiO|H$_2$SO$_4$|MWCNT and MWCNT-NiO|Na$_2$SO$_4$|MWCNT supercapacitor exhibits higher supercapacitive behaviour than their symmetry counterparts. The higher capacitive behaviour of the asymmetry (MWCNT-NiO|H$_2$SO$_4$|MWCNT) supercapacitor in comparison to its neutral counterpart (MWCNT-NiO|Na$_2$SO$_4$|MWCNT) can be attributed to the relatively smaller ionic size of the former which will allow easier diffusion through the electrode material pores. Its higher SC value compared with literature have also been attributed to the synergetic interaction between the synthesised NiO and the MWCNT, couple with the extent of the treatment of the MWCNT in acids. The electrode demonstrated high stabilities with no significant changes over 1000 cycles.

References

1. A.S. Adekunle, K.I. Ozoemena, *Electrochim. Acta* 53 (2008) 5774.
2. A.S. Adekunle, K.I. Ozoemena, *J. Solid State Electrochem.* 12 (2008) 1325.
3. B.E. Conway, *Electrochemical Super Capacitors*, Kluwer Academic/Plenum Publishers, New York, 1999.
4. M. Winter, R.J. Brodd, *Chem. Rev.* 104 (2004) 4245.
5. Y.H. Lee, K.H. An, J.Y. Lee, S.C. Lim, *Encycl. Nanosci. Nanotechnol.* 1 (2004) 625.
6. E. Frackowiak, F. Beguin, *Carbon* 40 (2002) 1775.
7. C. Du, J. Yeh, N. Pan, *Nanotechnology* 16 (2005) 350.
8. K.H. An, W.S. Kim, Y.S. Park, J.M. Moon, D.J. Bae, S.C. Lim, Y.S. Lee, Y.H. Lee, *Adv. Funct. Mater.* 11 (2001) 387.
9. S.H. Kim, Y.I. Kim, J.H. Park, J.M. Ko, *Int. J. Electrochem. Sci.*, 4 (2009) 1489.
10. J. Chen, N. Xia, T. Zhou, S. Tan, F. Jiang, D. Yuan, *Int. J. Electrochem. Sci.*, 4 (2009) 1063.
11. F. Lufrano, P. Staiti, Int. *J. Electrochem. Sci.*, 5 (2010) 903.
12. C. Portet, P.L. Taberna, P. Simon, E. Flahaut, *J. Power Sources* 139 (2005) 371.
13. F. Beguin, K. Szostak, G. Lota, E. Frackowiak, *Adv. Mater.* 17 (2005) 2380.
14. Z. Fan, J. Chen, K. Cui, F. Sun, Y. Xu, Y. Luang, *Electrochim. Acta* 52 (2007) 2959.
15. T. Shinomiya, V. Gupta, N. Miura, *Electrochim. Acta* 51 (2006) 4412.
16. G.Q. Zhang, S.T. Zhang, *J. Appl. Electrochem.* 39 (2009) 1033.
17. J. Wang, H. Qin, J. You, Z. Li, P. Yang, X. Jing, M. Zhang, Z. Jiang *J. Appl. Electrochem.* 39 (2009) 1803.
18. A.S. Adekunle, K.I. Ozoemena, *Electroanalysis* 23 (2011) 971
19. L. Cao, M. Lu, H.L. Li, *J. Electrochem. Soc.* 152 (2005) A871.
20. S.Y. Wang, K.C. HO, S.L. Kuo, N.L. Wu, *J. Electrochem. Soc.* 153 (2006) A75.
21. C-H. Hu, K-H. Chang, M-C. lin, Y-T. Wu, *Nano Letters* 6 (2006) 2690.
22. J.S. Ye, H.F. Cui, X. Liu, T.M. Lim, W.D. Zhang, F.S. Sheu, *Small* 1 (2005) 560.
23. Q.T. Qu, Y. Shi, S. Tian, Y.H. Chen, Y.P. Wu, R. Holze, *J. Power Sources* 194 (2009) 1222.
24. J.A. Liu, , G. Rinzler, H. Dai, J.H. Hanfer, R.K Bradley, P.J. Boul, A. Lu, T Iverson, K. Shelimov, C.B. Huffman, F.R. Macias, Y.S. Shon, T.R. Lee, D.T. Colbert, *Science* 280 (1998) 1253.
25. L. Xiang, X.Y. Deng, Y. Jin, *Scripta Mater.* 47 (2002) 219.
26. S.H. Wu, D.H. Chen, *J. Colloid Interf. Sci.* 259 (2003) 282
27. L. Xiang, X.Y. Deng, Y. Jin, *Scripta Mater.* 47 (2002) 219.
28. A.L.M. Reddy, S. Ramaprabhu, *J. Phys. Chem. C* 111 (2007) 7727.
29. V. Khomenko, E. Frackowiak, F. Beguin, *Electrochim. Acta* 50 (2005) 2499.
30. V. Ganesh, S. Pitchumani, V. Lakshminarayanan, *J. Power Sources* 158 (2006) 1523.
31. H.-Q. Wang, Z.-S. Li, Y.-G. Huang, Q.-Y. Li, X.-Y. Wang, *J. mater. Chem.*, 2010|DOI:10.1039/c000339e.
32. Q. Wang, Z. Wen, J. Li, *Adv. Funct. Mater.* 16 (2006) 2141.
33. C-W. Huang, Y-T. Wu, C-C. Hu, Y-Y. Li, *J. Power Sources* 172 (2007) 460.
34. B.J. Feldman, P. Burgmayer, R.W. Murray, *J. Am. Chem. Soc.* 107 (1985) 872.
35. N. Mermilliod, J. Tanguy, F. Petior, *J. Electrochem. Soc.* 133 (1986) 1073.
36. J. Tanguy, N. Mermilliuod, M. Hoclet, *J. Electrochem. Soc.* 134 (1987) 795.
37. T. Tanguy, M. Slama, M. Hoclet, J.L. Baudin, *Synth. Met.* 28 (1989) 145.
38. M. Kalaji, L.M. Peter, *J. Chem. Soc. Faraday Trans.* 87 (1991) 853.
39. X. Ren, P.G. Pickup, *J. Electroanal. Chem.* 372 (1994) 289.
40. G. Xu, W. Wang, X. Qu, Y. Yin, L. Chu, B. He, H. Wu, J. Fang, Y. Bao, L. Liang, *Eur. Polym. J.* doi:10.1016/j.europolymj.2009.05.016.
41. C. Du, N. Pan, *J. Power Sources* 160 (2006) 1487.

42. M.J. Green, N. Behabtu, M. Pasquali, W.W. Adams, *Polymer*
(doi:10.1016/j.polymer.2009.07.044).
43. S. G. Kandalkar, J. I. Gunjakar, C. D. Lokhande, *Appl. Surf. Sci*. 254 (2008) 5540.